World Journal of Chemical Education, 2021, Vol. 9, No. 1, 28-41
Available online at http://pubs.sciepub.com/wjce/9/1/5
Published by Science and Education Publishing
DOI:10.12691/wjce-9-1-5

Adsorptive Accumulation of Methylene Blue Dye from Aqueous Effluent by $NiFe_2O_4$-GO Nano-adsorbent

Taznur Ahmed[1], Susmita Sen Gupta[2,*]

[1]Department of chemistry, Science College Kokrajhar, Assam, India
[2]Department of chemistry, B N College Dhubri, Assam, India
*Corresponding author: ahmed.tazu@gmail.com

Received February 12, 2021; Revised March 18, 2021; Accepted March 26, 2021

Abstract In this article, the Methylene Blue dye adsorption is studied using $NiFe_2O_4$-Graphene Oxide composite as adsorbent. The $NiFe_2O_4$-graphene oxide ($NiFe_2O_4$-GO) nano-composite made by single step solvothermal approach. The characterization study revealed the abundance of functional group and nanomaterial features in prepared material. The MB adsorption is increased with rising adsorbent doses, pH, temperature and initial MB solution concentrations. Pseudo second order kinetic model got fitted by adsorption kinetics. As compared to BET, Temkin, Freundlich and Dubinin-Radushkevich model, Langmuir model is suitable for adsorption isotherm. Thermodynamic studies suggest adsorption process's endothermic nature and spontaneity. The adsorption advances through π-π interaction, H-bonding and electrostatic attraction. Reusability study reveals the prepared adsorbent is a promising as well as cost effective sorbent for high efficiency and excellent renewability.

Keywords: *Adsorption, $NiFe_2O_4$-GO composite, Methylene Blue, kinetics, isotherms*

Cite This Article: Taznur Ahmed, and Susmita Sen Gupta, "Adsorptive Accumulation of Methylene Blue Dye from Aqueous Effluent by $NiFe_2O_4$-GO Nano-adsorbent." *World Journal of Chemical Education*, vol. 9, no. 1 (2021): 28-41. doi: 10.12691/wjce-9-1-5.

1. Introduction

The basic dye, Methylene Blue (MB) (tetra-methylthionine chloride) has been utilized in microbiologic as well as histologic staining. Its clinical use is done in methemoglobinemia treatment [1]. However, the toxic effect of MB had also been reported in a neonate [2] and results in acute renal failure, hyperbilirubinemia, hemolytic anemia, parathyroid adenoma [3], Alzheimer's disease [4] etc.

Many chemicals are defiant to processing of predictable treatment, like simple biological, chemical and physical water refinement strategies. Such issues draw the attention of researchers to develop novel carbonaceous nano adsorbent for advance water treatment [5,6,7] via developing and implementation of various approaches for the contaminants removal from waste water.

Vast applications for the graphene-family nanomaterials were reported. It has the similar graphite structure that consists of (a) few-layer graphene (b) reduced GO(rGO) with a few oxygen groups (c) graphene oxide(GO) containing hydroxyl, carbonyl, epoxide, as well as carboxyl functional groups on the surface and/or on the edges [8]. The nanomaterials of graphene-family exhibit excellent properties like mechanical strength, electrical conductivity and for organic/inorganic contaminant's high adsorption capacity [9]. The usage of nanomaterials of graphene family for adsorption required a great energy deal from aqueous solutions for recovering or reusing them [10]. To overcome such problems, spinel ferrites (MFe_2O_4, where M=Mn, Ni, Zn, Cu, Co, etc.) will be combined as interior materials in nanomaterials of graphene-family. The ferrites fascinated a great interest because of their extraordinary electrical, catalytic, and magnetic properties which have potential usefulness for varied practical applications [11].

The ferrites in the interior of the graphene nano-sheets resist the agglomeration, whereas toxic substance leaching are restricted by the graphene and adsorption properties are enhanced through a particular chemical stability and large surface area. The graphene nano-sheets associated with magnetic ferrites (GNSF) provide additional advantages of easy recovery of the adsorbent after removing and reusing contaminants by utilizing an external magnetic field. This study critically highlighted the application of GNSFs as specific nano adsorbents for removal of MB from aqueous solution.

2. Materials and Methods

2.1. Materials

Graphite powder, H_3PO_4, H_2SO_4, ethylene glycol(EG), NaOH, $Ni(NO_3)_2.6H_2O$, $Fe(NO_3)_3.9H_2O$, EtOH, Methylene Blue (Molecular formula: $C_{16}H_{18}Cl\ N_3S$, CI Classification Number: 52015, Figure S1)(Mark chemical laboratory reagent Co. Ltd., Mumbai) chemicals of analytical grade were used without purification.

2.2. Synthesis of Adsorbent

2.2.1. Preparation of Graphene Oxide (GO)

The main precursor GO was prepared by using modified Hummer process [12], 1.5g Graphite flakes and 9.0g $KMnO_4$ added successfully into a mixture of conc. H_3PO_4 and conc. H_2SO_4 of ratio 1:9 by volume under unremitting stirring for 12hrs at 323K. The mixture was cooled and poured slowly below dynamic stirring into ice chilled beaker containing H_2O_2 (30%), the mixture was washed with 30% ethanol and HCl at 350°C.

2.2.2. Preparation of $NiFe_2O_4$-Graphene Oxide (NFO-GO) Composite

Synthesized GO (0.9g) is exfoliated in 80mL of EG by ultrasonication for more than 3hrs. 1.5g of NaOH, 0.95g of $Ni(NO_3)_2.6H_2O$ and 1.72g of $Fe(NO_3)_3.9H_2O$ are dissolved at ambient temperature in solution of GO-EG. After careful stirring for 30mins, the solution is shifted to 100mL stainless-steel teflon-lined autoclave to preserved at 473K for 6hrs and then the mixture is cooled to normal temperature. A black precipitate obtained, washed, centrifuged many times using EtOH. Lastly, the materials extracted is dried at 333K in a vacuum oven [13].

2.3. Dye Adsorption

Batch adsorption methodology followed for the dye removal experiment. The predetermined adsorbent amount is mixed with 50mL dye solution in 100mL conical flask and allowed to shaken in thermostated water bath shaker (ISO 9001:2008; SUPERIOR SCIENTIFIC INDUSTRIES) for specific period of time. At presets interval of time, centrifugation used for separation of solution from the mixture. The Visible spectrometer is used to measure adsorbed dye's concentration in supernatant solution (Elico SL 177). Furthermore, mass balanced equation is used for calculating adsorption extent (%) and dye adsorbed per unit adsorbent mass(q).

$$q = \frac{(C_o - C_e)V}{m} \quad (1)$$

$$\text{Adsorption Extent}(\%) = \left[\frac{(C_o - C_e)}{C_o}\right]100 \quad (2)$$

where, q(mgg^{-1}) is the adsorbate amount adsorbed per mass(g) of adsorbent. C_0(mgL^{-1}) and C_e(mgL^{-1}) are dye's initial and equilibrium concentration. V(L) is solution's volume of experiment and m(g) is adsorbent's mass.

The process of adsorption presented under solution temperature, pH, interaction time, adsorbent load, and initial dye concentrations at diverse experimental condition (Table 1). The adsorbent's reusability investigation carried out subsequent to loaded adsorbent's desorption for the adsorption capacity.

2.4. Characterization of Adsorbent

The investigation of powdered XRD pattern carried out in Bruker AXS(Germany) "X-ray powder diffractometer Model D8", which focus on Cu Kα monochromatized radiation which has 0.02°(2θ) step size as well as 0.15418nm wavelength. The determination of NFO-GO composite's pore volume, pore diameter and particular surface area were executed by Brunauer-Emmet-Teller (BET) N_2 gas approaches by utilizing automated gas sorption analyser (Quantachrome® ASiQwin™ Instrument, NOVA-1000 version 3.70). The analysis of morphology (FESEM images) and elemental study (EDX) is achieved using Carl Zeiss (Germany) SUPRA 55VP, Gemini Column with air lock system model. Laser Raman microscope (Labram HR Evolution, Horiba) is used to get the Raman spectra. The X-ray photoelectron spectroscopy (XPS) measurement is carried out in X-ray photoelectron spectrometer Multilab2000. The Zeta sizer, Malvern is used to measure zeta potentials and the charges nature on surface. The Differential scanning calorimetry (DSC) analysis and Thermogravimetric (TG) analysis are studied out in DSC1 Star System Mettler Toledo model to study the thermal stability.

Table 1. Experimental conditions for Adsorption Study

Sl no.	Parameter for adsorption process	Experimental set-up
1	Effect of time	adsorbent 0.2 gL^{-1}, dye concentration 10 mgL^{-1}, pH 7.19, temperature 303K, time 10 - 240 min
2	Effect of dye concentration	adsorbent 0.2 gL^{-1}, pH 7.19, time 240 min, temperature 303 K, dye concentration 10-30 mgL^{-1}
3	Effect of adsorbent load	dye concentration 10 mgL^{-1}, pH 7.19, temperature 303 K, time 240 min, adsorbent 0.08 - 0.36 gL^{-1}
4	Effect of pH	adsorbent 0.2 gL^{-1}, dye concentration 10 mgL^{-1}, temperature 303 K, time 240 min, pH 2.0- 12.0
5	Effect of temperature	adsorbent 0.2 gL^{-1}, dye concentration 10 mgL^{-1}, time 240 min, pH 6.5, temperature 303 K - 333K

3. Result and Discussion

3.1. Characterization of adsorbents

3.1.1. X-Ray Diffraction Pattern (XRD) Analysis

XRD patterns of $NiFe_2O_4$ (NFO) and $NiFe_2O_4$-Graphene oxide composite (NFO-GO) was published elsewhere [13] (Figure S2). NFO-GO represented wide peak at 25.1° (2θ) with the inter planar spacing of 0.36nm, might be due to (002) plane for GO. Crystals sizes of 11.48nm, 5.72nm, 6.99nm, 7.02nm and 12.84nm were obtained from Scherrer equation (D_p=0.94λ/($\beta_{1/2}$Cosθ, where $\beta_{1/2}$= width at X-ray line broadening reflection's half maximum, θ =diffraction angle, λ= Cu K_α radiation's wavelength [14].

3.1.2. Field Emission Scanning Electron Microgram (FESEM) and EDX Analysis

FESEM images (Figure 1A) clearly indicated the association of NFO particles in the GO sheet preventing GO sheet from agglomeration and make easy to peel off by ultrasonication. The figure indicated that GO sheets are separated largely by the introduction of NFO particles.

The EDX (Figure 1B) analysis confirmed the presence of carbon, oxygen, iron and nickel elements in NFO-GO nano-composites [15].

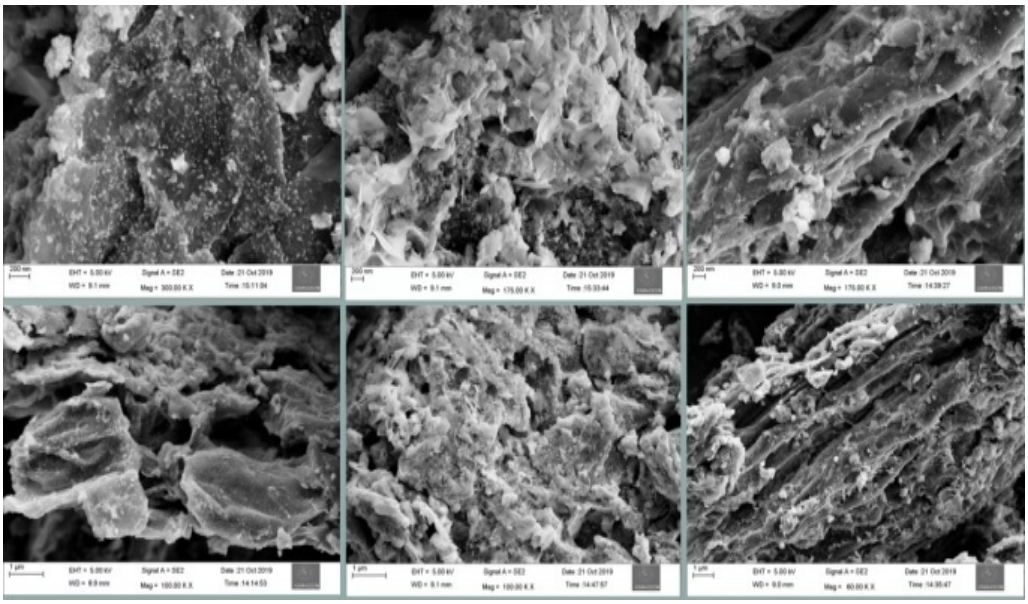

Figure 1A. FESEM images of NFO-GO composite

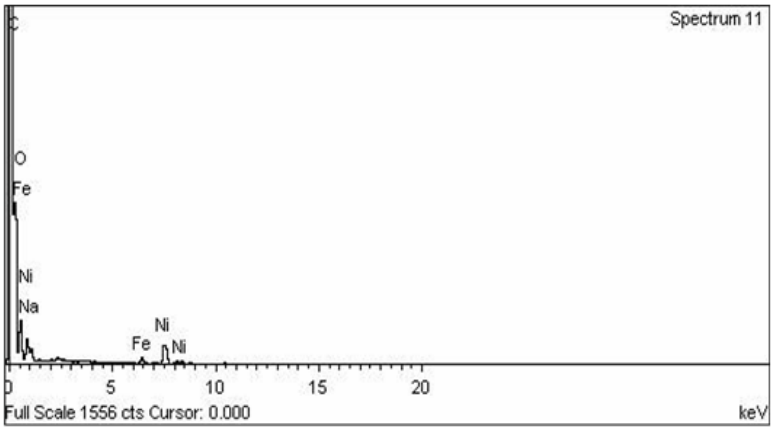

Figure 1B. EDX spectra of NFO-GO composite

3.1.3. Raman Spectra Analysis

Raman spectra of NFO-GO (Figure 2) displayed noticeable peaks at 1598.55cm^{-1} and 1341.08cm^{-1} for two (G and D) bands. Assignment of G band is preferred for E_{2g} mode which observes sp^2-carbon domain while structural disorders and defects are connected through D band which results in breaking selection rule as well as symmetry [16]. The intensity ratio(I_D/I_G) utilized to measure the disorder [17] and found to be 1.002 showed an enhanced value indicating localized sp^3 defects within the sp^2 carbon network indicated the successful oxidation of graphene. The Raman spectra also exhibits five Raman bands [18] typically for the inverse spinel structure of $NiFe_2O_4$. The group theoretical calculation shows five Raman band $A_{1g}+E_g+3T_{2g}$ for $NiFe_2O_4$ crystal of space group Fd-3m [19].

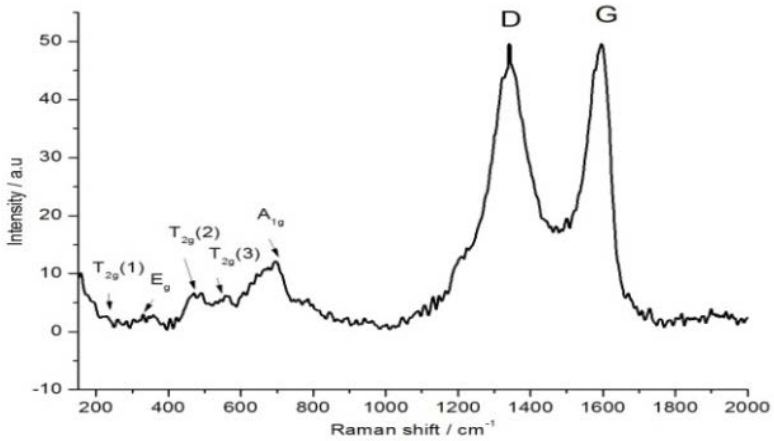

Figure 2. Raman spectrum of NFO-GO composite

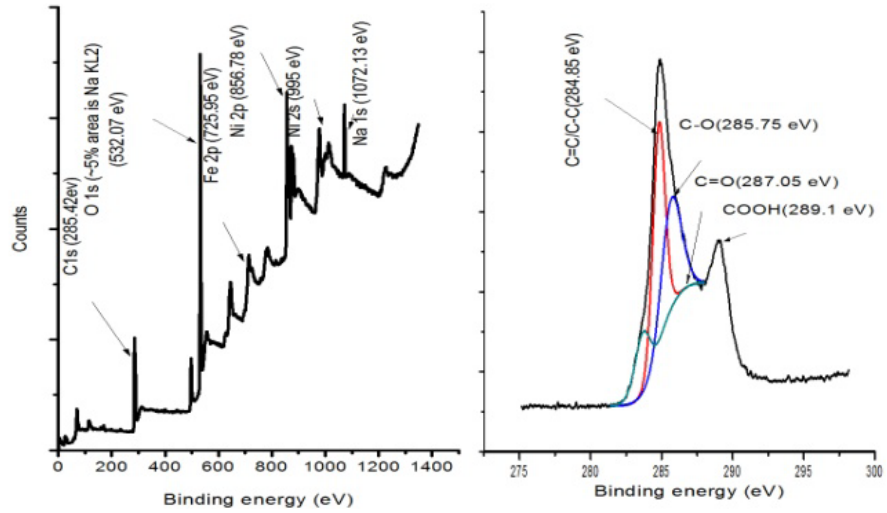

Figure 3. X-ray photoelectron spectra of C 1s in NFO-GO composite.

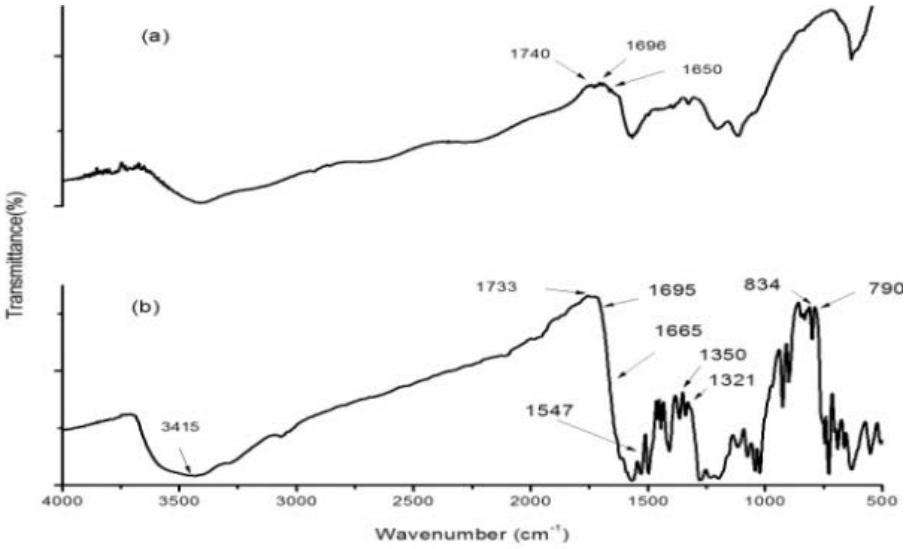

Figure 4. FT-IR spectra (a) $NiFe_2O_4$-GO composite (b) MB loaded $NiFe_2O_4$-GO composite

3.1.4. X-ray Photoelectron Spectroscopy Analysis

The literature of XPS analysis revealed that GO consists of two main peak, hydrophobic π- conjugated sp^2 domain and hydrophilic oxygen containing functional groups with sp^3 domain [20]. The full screen XPS spectrum (Figure 3) exhibited the presence of C, O, Fe and Ni elements at the binding energy 285.42eV, 532.07eV, 725.95eV and 856.78eV respectively. The Carbon/Oxygen content implied that a greater number of oxygen containing group successfully introduced into the prepared composites. A computational multi peak resolution methods of C1s band deconvoluted into four peaks at 284.85eV, 285.75eV, 287.05eV and 289.01eV, resulting C=C/C-C, C-O, C=O and COOH groups respectively [21]. FT-IR spectra (Figure 4) supported the report obtained in XPS analysis.

3.1.5. Adsorbent's Surface Area Determination

At high relative pressure, BET plots indicate type-I for wider hysteresis loop of isotherm by IUPAC classification [13] (Figure S3, published elsewhere), the isotherm's feature discovered that with narrow slit pores high adsorption performance is presented by NFO-GO composite.

BET specific surface area of 88.027m^2g^{-1} with pore diameter 3.48nm and pore volume 0.131ccg^{-1} indicate an impressive result as adsorbent whereas the reported GO's specific surface area is 31.4m^2g^{-1} [22].

3.1.6. Adsorbent's Surface charge Determination

At 5.0 to 9.0pH range Zeta potential's measurement estimate no zero point charge of NFO-GO indicating the adsorbent's negative surface charge (Figure 5).

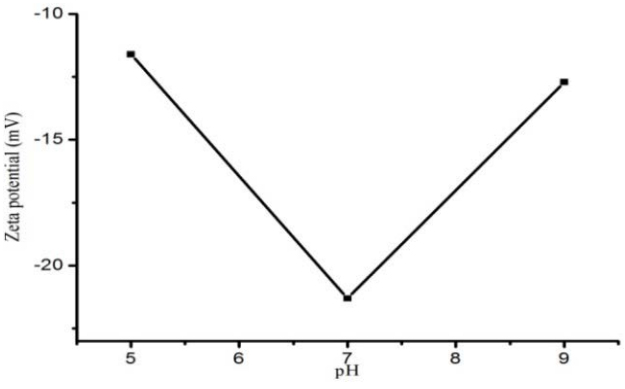

Figure 5. Zeta potential variation with solution pH

3.1.7. Thermal Stability Analysis of Adsorbents

Thermogravimetric analysis of NFO-GO presented that approximately 10% weight loss observed to 373K, might be due to water vapor's loss. In 373K-800K temperature range 16% weight loss occurs that might be because of carbon-oxidation [23]. After oxidations, nearly ~74% weight is related to NFO-GO weight. In DSC curve an endothermic peak was observed at nearly 385K attributing to glass transition temperature (Figure 6).

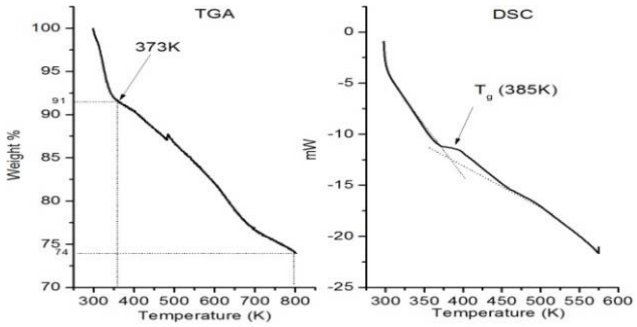

Figure 6. Thermogravimetric analysis of NFO-GO composite

3.2. Dye Adsorption Study

3.2.1. Influence of Contact Time

The contact time effect for Methylene Blue adsorption on NFO-GO is achieved at various temperatures (303- 333K).

MB adsorption (303K) per unit mass of adsorbent is enhanced from 39.28mgg^{-1} (10min) to 48.15mgg^{-1} (240min) steadily (Figure S4). However, for NFO, the maximum value of q_e(303K) is 1.4mgg^{-1}(240min). At beginning, maximum adsorption has taken place and equilibrium attained by slowing down within 240 min. At initial periods high adsorption capacity might be because of enormous active sites that encourage the dye molecule in proficient adsorbent attachment. Adsorption equilibriums was attained due to saturation of binding site [24,25].

3.2.2. Influence of pH

Negatively charged surface of adsorbent may compete for proton along with the dye molecules thus the adsorption process increases with increasing pH of the solution (Figure S5). The electrostatic attraction between cationic MB with NFO-GO composite increases with pH [26]. Therefore, the adsorbent's negative surface attracts the dye molecule very easily that supported by Zeta potential values.

3.2.3. Influence of Solution Concentration

The adsorption of MB per unit adsorbent's mass enhanced from 48.15mgg^{-1} to 97.37mgg^{-1} at 303K with the concentration of dye from 10mgL^{-1} to 30mgL^{-1} (Figure S6). The dye's mass transfer resistance between the solid phase and the aqueous phase is overcome by providing higher driving force via enhancing the dye concentration which results more collision among adsorbent's solid phase and dye molecule. At the higher dye concentration, adsorbent's mass is exposed to thousands dye species and appropriate binding sites are gradually filled by the dye's progressive high numbers. It results in q_e enhancement, however, there is declination in the net adsorption [27].

3.2.4. Influence of Adsorbents Dosage

There exists a reduction in adsorption capacity (q_e) when adsorbent amount is increased from 0.08gL^{-1} to 0.36gL^{-1}. However, the extent of adsorption presented a gradual increase as adsorbents load increases (Figure S7).

The enhancement of extent of adsorption may be because of surface negative charge enhancement as well as electrostatic potential reduction near the solid surfaces that favours adsorbent-adsobate interaction. While, the greater adsorbent amount efficiently decreased the unsaturations of adsorption sites due to overcrowding and correspondingly such sites per unit mass decreases which results in reasonably low adsorption capacity(q_e) at higher dosage of adsorbent [28,29]. Moreover, adsorption sites are easily accessed by the dye species in less adsorbent amount.

3.2.5. Influence of Temperature

MB adsorption capacity is increased with rise in temperature from 303K to 333K indicating endothermic nature of adsorbent-dye interaction (Figure 7). Increase in temperature might result porosity swelling that enabled the adsorbate molecule to quick diffusion into NFO-GO composites pores as well as into the external boundary layer [30,31]. The increase in adsorption capacity of MB is preferred by temperature rise and an activation energy provided more driving force in overcoming such energy barrier to get surface attachment [32].

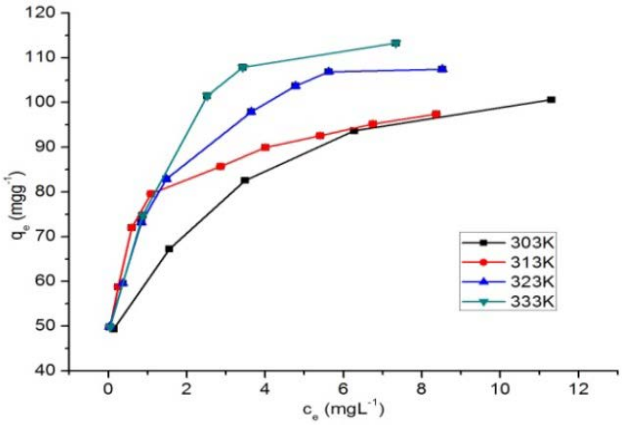

Figure 7. Variation of q_e Vs C_e plots at different temperature

3.2.6. Kinetics study

3.2.6.1. Pseudo First and Pseudo Second Order Kinetics Model

Pseudo first order kinetic [33] and pseudo second order kinetic [34] is widely used in adsorption phenomenon as

$$\log(q_e - q_t) = \log q_e - K_1 t / 2.303 \quad (3)$$

$$\frac{t}{q_t} = \frac{1}{K_2 q_e^{\,2}} + \frac{t}{q_e} \quad (4)$$

where, q_e and q_t is MB adsorbed(mgg^{-1}) at equilibrium and at time t(min) respectively. The linearity of the

curve log (q_e - q_t) Vs t and t/q_t Vs t represents pseudo first order and pseudo second order kinetic models (Figure 8) respectively. K_1(min^{-1}) and K_2 ($gmg^{-1}min^{-1}$) is the first order and second order rate constant respectively.

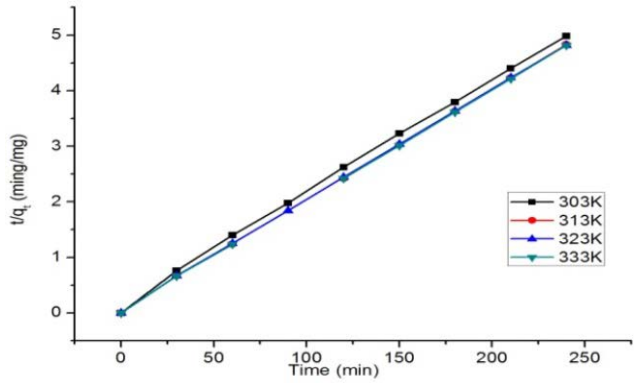

Figure 8. Pseudo second order plots of MB adsorption onto NFO-GO composite

The value of adsorption capacity calculated ($q_{e,cal.}$) for pseudo first order model differed from experimental data ($q_{e,exp.}$) with a deviation of -69.94%. However, the deviation for pseudo second order model is relatively small (1.29%), suggesting the closeness of experimental value to theoretical value. The minute deviations observed in pseudo second order model might be because of experimental error. Table 2 summarizes the information attained at various temperatures from pseudo second order model.

3.2.6.2. Elovich Kinetics Model

The Elovich kinetic model[35] applied to the adsorption phenomenon considering that (i) The adsorbent surface is energetically heterogeneous and (ii) At the low surface coverage adsorbed dyes neither interacted nor desorpted that can significantly affect the adsorption kinetic. The Elovich equation is

$$q_t = \left(1/\beta\right)\ln\left(\alpha\beta\right) + \left(1/\beta\right)\ln t \qquad (5)$$

The parameter α and β are the initial rate and Elovich constant respectively. The calculated plot values for co-efficient correlation, α(adsorption co-efficient) and β(desorption co-efficient) at different experimental temperature are tabulated in Table 2.

3.2.6.3. Intra-particle Diffusion Model

In the process of solid/liquid sorption the solute transfer may consist of either the mass transfer step (film diffusion) or diffusion of intra-particle or both. The diffusion mechanism of dye removal from aqueous solution by adsorption is multi-step process [36]. For porous adsorbent, dye molecule's diffusion into the adsorbent's pores cannot be denied. Therefore, this model is also considered in finding out the reasonable adsorption kinetic model [37]. Weber and Morris simplified the intra-particle diffusion model [38] and can be expressed as-

$$q_t = k_i t^{0.5} + C \qquad (6)$$

k_i ($mgg^{-1}min^{0.5}$) represented the rate of intra-particle diffusions. The data attained for rate constant (k_i) is $2.67mgg^{-1}min^{0.5}$ at i-stage, The intercept(C) suggested the boundary layer thickness. The non-linearity of the q_t v$_s$ $t^{0.5}$ curve indicated that diffusion of intra-particle may not have substantial part in the overall process of dye adsorption.

The q_t V$_s$ $t^{0.5}$ plots (Figure 9) are multilinear consisting three linear segments. The 1st segments with great slope due to MB transport to NFO-GO composite's external surface from solution. The 2ndsegment explains the steady adsorption stage corresponds to MB molecule's diffusion into the adsorbent's pore from the external surface (intra-particle diffusion). The 3rd segment with small slope describes the stage of final equilibrium in which diffusion of intra-particle initiates to decrease.

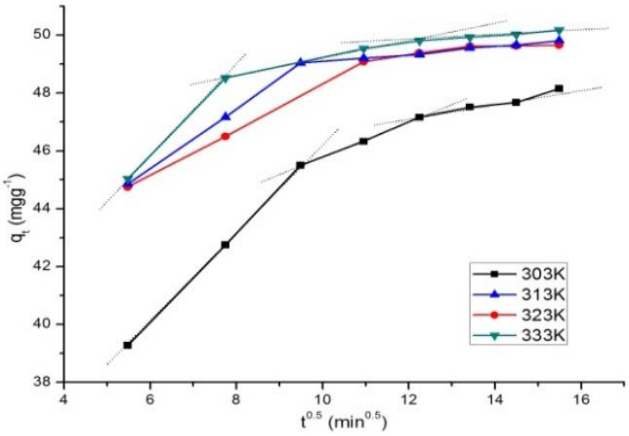

Figure 9. Intraparticle diffusion model of MB adsorption onto NFO-GO composite

The non-zero value of the intercept(C) for every linear segment (Table 2) indicating that the intra-particle diffusion is not the only controlling rate step in every stage in diffusion process [39]. Once the solute particles are loaded, the sorption process is controlled by intra-particle diffusion.

3.2.6.4. Boyd's Film Diffusion Model

Boyd's model is used for analyzing the experimental data [40] to get insight into adsorption process's actual rate controlling step.

$$B_t = -0.4977 - \ln\left(1-F\right) \qquad (7)$$

Where, F is the equilibrium's fractional attainment at various time (t) and B_t represented F's mathematical function.

$$F = q_t / q_e \qquad (8)$$

Thus, B_t value could be measured from equation (7). The linearity of the plot indicated consistent information that the adsorption rate is controlled by transfer of external mass (film diffusion) phenomenon. At initial stage, the plot of calculated B_t Vs t did not pass through the origin indicating adsorption rate controlled by film diffusion and subsequently switch to other mechanism like intra-particle diffusion.

Table 2. Kinetic parameters for the MB adsorption

C_0 (mgL^{-1})	**Pseudo first-order kinetics**					
	Temperature(K)	$K_1(min^{-1})$	$q_{e,\,cal.}(mg\ g^{-1})$	$q_{e,\,exp.}(mg\ g^{-1})$	Deviation (%)	R^2
	303	1.57×10^{-2}	13.92	48.15	-69.64	0.967
	313	3.06×10^{-2}	6.67	49.65	-86.56	0.867
	323	1.63×10^{-2}	5.61	49.82	-88.7	0.927
	333	3.88×10^{-2}	15.889	50.18	-68.33	0.940
	Pseudo second-order kinetics					
	Temperature(K)	$K_2(g\ mg^{-1}\ min^{-1})$	$q_{e,\,cal.}(mg\ g^{-1})$	$q_{e,\,exp.}(mg\ g^{-1})$	Deviation (%)	R^2
	303	4.59×10^{-3}	48.78	48.15	1.30%	0.999
	313	7.23×10^{-3}	50.02	49.65	0.75%	0.999
	323	1.04×10^{-2}	50.10	49.82	0.56%	0.999
	333	1.46×10^{-2}	50.20	50.18	0.03%	0.999
10	**Elovich kinetics**					
	Temperature(K)	α (adsorption co-efficient) (mgg^{-1})		β (desorption co-efficient) ($mingmg^{-1}$)		R^2
	303	1.87×10^{3}		2.39×10^{-1}		0.968
	313	9.28×10^{7}		4.57×10^{-1}		0.779
	323	5.25×10^{7}		4.46×10^{-1}		0.853
	333	4.75×10^{7}		4.41×10^{-1}		0.852
	Intraparticle diffusion kinetics					
	Temperature(K)	K_1	K_2	K_3	C_1	C_2	C_3	$(R_1)^2$	$(R_2)^2$	$(R_3)^2$
	303	1.550	0.601	0.288	30.76	39.77	43.61	0.999	0.997	0.943
	313	0.792	0.214	0.019	40.40	46.74	49.35	0.999	0.997	0.944
	323	1.040	0.132	0.123	39.15	47.74	47.89	0.999	0.911	0.960
	333	1.535	0.291	0.112	36.63	46.29	48.44	0.999	0.986	0.981

3.2.7. Adsorption Isotherm

Chemical species accumulation is allowed by the adsorption into the adsorbent's solid phase as well as into their interfaces. Empirical isotherm models provide information related to experimental findings. BET, Dubinin-Radushkevich, Temkin, Freundlich, and Langmuir isotherm model are used to get insight the adsorption process.

3.2.7.1. Langmuir and Freundlich Isotherm

The linear form of Freundlich [41] and Langmuir [42] equation can be expressed as-

$$\log(q_e) = \log k_f + \log(c_e)/n \tag{9}$$

$$\frac{c_e}{q_e} = \frac{c_e}{q_m} + \frac{1}{bq_m} \tag{10}$$

Where, $c_e(mgL^{-1})$ =equilibrium concentration of MB solution, $q_e(mgg^{-1})$=equilibrium adsorption capacity, $q_m(mgg^{-1})$= Langmuir maximum adsorption capacity corresponds to total coverage of monolayer, b = Langmuir constant to binding site's affinity as well as adsorption energy, $k_f(mg^{1-1/n}\ L^{1/n}g^{-1})$ =Freundlich constant related to capacity of adsorption, 1/n =factor of heterogeneity indicating adsorption process's feasibility.

The linear relation between c_e/q_e Vs c_e plots (Figure 10) indicated the adsorption process obey Langmuir isotherm model. Table 3 listed the correlation coefficients and isotherm values. q_m and b increased with enhancement of temperature due to the endothermic nature of adsorption process [43]. Other important parameter R_L [44], a dimensionless separation constant can be represented as-

$$R_L = \frac{1}{1 + bC_o} \tag{11}$$

Where, c_o represented maximum initial concentration of MB (mg/L). The separation constant specified that the isotherm is favourable for $R_L<1$, not favourable for $R_L>1$, linear for $R_L=1$ and irreversible for $R_L=0$ [45,46]. The R_L value in between 0.007 to 0.02 indicating the adsorption process is favourable.

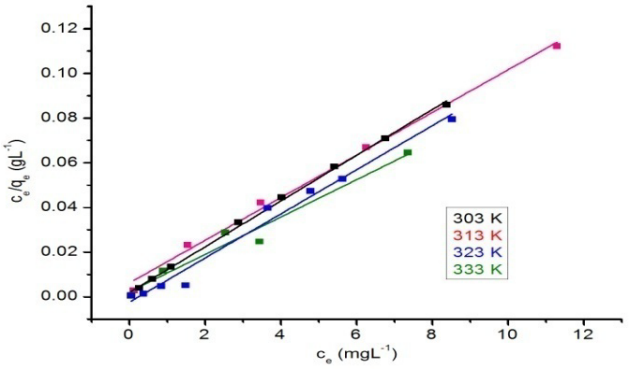

Figure 10. Langmuir isotherm model of MB adsorption onto NFO-GO composite

The examination of linear fitting curve of $\log q_e$ Vs $\log c_e$ for Freundlich isotherm (equation 9) showed that the correlation co-efficient (R^2) value is much less than that of Langmuir isotherm curve (Table 3), although it increased with increasing temperature.

As compared to Freundlich isotherm model, Langmuir isotherm model fitted better with experimental value. The monolayer Langmuir adsorption capacity is measured as $97.94mgg^{-1}$ for MB.

3.2.7.2. Temkin Isotherm

It assumed that heat of the molecules reduces with coverage due to adsorbent-adsorbate interaction. Temkin

Isotherm model explained in linear form [47] in adsorption as-

$$q_e = 2.303RT / b_T \log\left(A_T - \log C_e\right) \quad (12)$$

where, T= solution temperature(K), R($JK^{-1}mol^{-1}$)= gas constant, A_T(g^{-1})= equilibrium binding constant consistent to maximum binding energy, RT/b_T=B ($Jmol^{-1}$) represented Temkin constant corresponding to sorption. The linear fitting of q_eVs $logc_e$ curve for MB monolayer adsorption on NFO-GO revealed the R^2= 0.929.

3.2.7.3. Dubinin-Radushkevich Isotherm

The Dubunin-Rudushkevich (D-R) Isotherm play significant part for the porous adsorbent, characteristics with wide variety of pore shape and sizes [48]. The linear form of D-R isotherm and desorption energy equation is given by [49]-

$$\ln q_e = \ln q_s - K_{dr}\varepsilon^2 \quad (13)$$

$$E = \left(2K_{dr}\right)^{-0.5} \quad (14)$$

Where, E($kJmol^{-1}$)= adsorbate's energy per molecule for eliminating a molecule to infinity from its sorption site's location, ε=Polanyi potential [ε=RTln(1+1/C_e)], K_{dr}(mol^2/J^2) = D-R isotherm constant linked with free energy, q_s(mgg^{-1}) = D-R theoretical saturation capacity. The parameter values (Table 3) from lnq_e Vs ε^2 linear fitting curve for D-R Isotherm(Figure S8) is q_s= 85.86mgg^{-1} and E= 8.3$kJmol^{-1}$. It recommended the MB's physical adsorption on adsorbent.

Table 3. Correlation coefficient for the adsorption isotherm

Isotherm	Parameters	Temperature			
		303 K	313 K	323 K	333 K
Langmuir	q_m (mg g^{-1})	97.465	104.6	107.41	114.94
	b	2.33	1.6	5.96	4.14
	R^2	0.987	0.992	0.995	0.986
	R_L	0.014	0.020	0.00 6	0.007
Freundlich	k_f($mg^{1-1/n}L^{1/n}g^{-1}$)	69.44	77.6	78.82	85.03
	n	4.57	6.67	6.43	6.94
	R^2	0.8002	0.948	0.927	0.886
Tempkin	A_T (g^{-1})	369.15	1267.63	3873.7	2605.4
	B ($Jmol^{-1}$)	11.77	11.27	9.41	11.23
	R^2	0.929	0.906	0.9682	0.891
D - R	q_s(mgg^{-1})	85.86	86.02	89.73	101.88
	E ($kJmol^{-1}$)	8.3	5.1	7.9	7.3
	R^2	0.695	0.680	0.552	0.885
BET	q_m (mgg^{-1})	70.61	71.84	81.10	86.45
	Kb	99.73	1712.97	154.54	314.79
	R^2	0.998	0.996	0.992	0.988

3.2.7.4. BET Adsorption Isotherm

BET adsorption model is dependent on the statement that there are chances that onto the adsorbent surface adsorbate will be adsorbed causing multi layer formation in adsorbed dye's random distribution [50]. It has been assumed that the condensation energy as well as adsorption energy are the reason for the successive layer's adsorption as well as for the first monolayer respectively. The BET equation's linear form [51] is-

$$\frac{c_e}{\left(c_o - c_e\right)q_e} = \frac{c_e\left(K_b - 1\right)}{K_b q_m c_o} + \frac{1}{K_b q_m} \quad (15)$$

Where, K_b= BET constant, $q_{m=}$ adsorbate amount that forms total monolayer (mgg^{-1}), q_e represents adsorbate amount adsorbed onto adsorbent(mgg^{-1}), c_o represents adsorbate's saturation concentration (mgL^{-1}), c_e represents adsorbate's equilibrium concentration(mgL^{-1}) in solution. The plots of $\frac{c_e}{\left(c_o - c_e\right)q_e}$ Vs c_e/c_o at various temperature are plotted (Figure S9) and calculated monolayer capacity are listed in Table 3. The parameters indicated the multilayer formation of MB-NFO-GO interaction.

3.3. Thermodynamic Study

The thermodynamics parameters, namely, Gibb's free energy (ΔG), entropy(ΔS) and enthalpy (ΔH) for dye adsorption are measured by following equation [52].

$$\ln K_d = \Delta S/R - \Delta H/RT \quad (16)$$

$$\Delta G = \Delta H - T\Delta S \quad (17)$$

where, R= ideal gas constant(8.314 $JK^{-1}mol^{-1}$), T= temperature (K), K_d(q_e/c_e)= distribution coefficient.

In order to calculate the adsorption's activation energy Arrhenius equation applied as-

$$\log K_2 = \log A - E_a/2.303RT \quad (18)$$

where, A= Arrhenius factor, E_a($kJmol^{-1}$)= Arrhenius activation energy, and K_2($gmg^{-1}min^{-1}$)= pseudo second order rate constant.

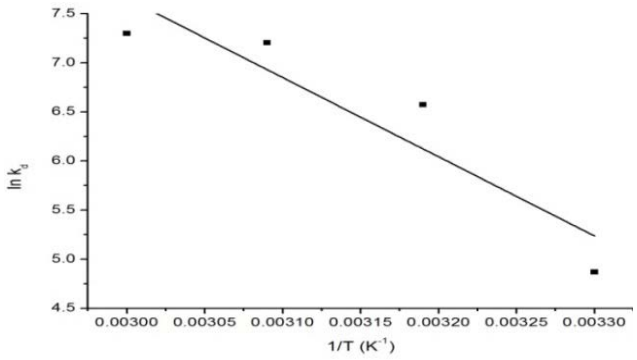

Figure 11. Plots for thermodynamics study.

The slope and intercept from linear plot of lnK_dVs 1/T is used for calculating ΔH and ΔS values (Figure 11, Table 4). The positive value of ΔH recommended the endothermic adsorbate-adsorbent interaction. The rise of randomness is indicated by positive value of ΔS which might be due to the structural changes of adsorbent in adsorption process.

Gibb's negative free energy (ΔG) decreased from -13.17$kJmol^{-1}$ to -21.11$kJmol^{-1}$ with rise in temperature (303K-333K). MB adsorption process's spontaneity is

more positive at high temperature [53]. Depending on ΔG value, MB's adsorption onto NFO-GO thought to be involving physisorption [50].

The Arrhenius parameter was determined by linear fitting curve of $logK_2$ Vs 1/T (equation 18) offered the $-E_a/2.303R$ slope and logA intercept (Figure 12). For activation energy result attained is 33.458 $kJmol^{-1}$ which indicates the process of adsorption may be controlled physically [54].

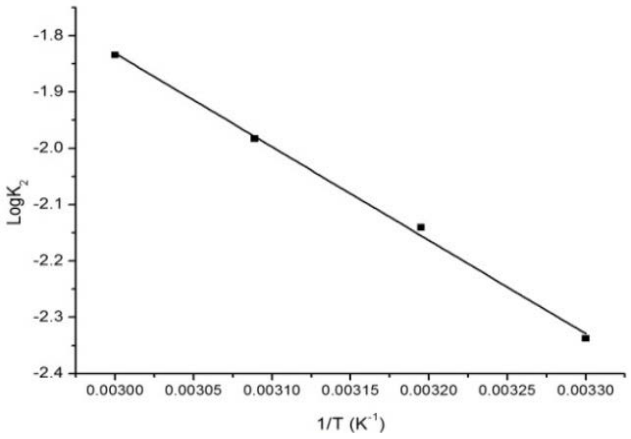

Figure 12. Arrhenius plots of MB adsorption onto NFO-GO composite

Table 4. Thermodynamic data for dye adsorption

ΔH ($KJmol^{-1}$)	ΔS ($JK^{-1}mol^{-1}$)	E_a ($kJ\ mol^{-1}$)	ΔG($kJK^{-1}mol^{-1}$)			
			303K	313K	323K	333K
+67.066	+264.8	33.458	-13.17	-15.82	-18.46	-21.11

3.4. Adsorption Mechanism

The pH influence for MB adsorption suggested that the electrostatic attraction could be the prime adsorption force. Although the process of adsorption observed to occur through a complicated adsorption mechanism where various interaction types might be involve in adsorption of MB onto NFO-GO composites. Investigation of FT-IR spectrums (Figure 4) of MB loaded NFO-GO and NFO-GO are carried out for verifying the adsorption process mechanism. The FT-IR spectra of MB loaded NFO-GO showed various changes. Adsorption band at $1696cm^{-1}$ and $1735cm^{-1}$ in NFO-GO composite conforming C=O and COOH slightly shifted to $1695cm^{-1}$ and $1733cm^{-1}$ respectively, indicating that the carboxylic group has significant role in the adsorption process. It might be because of the ionization of carboxylic group that made NFO-GO composite surfaces negatively charged. The adsorption peak at $1650cm^{-1}$ and $3427cm^{-1}$ belong to C=C and O-H shifted to $1677cm^{-1}$ and $3415cm^{-1}$ respectively, suggest that hydrogen bond and π=π interaction could contribute MB adsorption [55,56]. The characteristic adsorption peaks for aromatic rings system at $834cm^{-1}$, $790cm^{-1}$ and $1547cm^{-1}$ confirmed π-π interaction of the carbon atom of NFO-GO with B molecules which contain C=C double bond as well as benzene ring [57]. The C-N stretching frequency at $1350cm^{-1}$ and $1321cm^{-1}$ confirms the hydrogen bond existence between MB's nitrogen and NFO- GO's hydroxyl [58].

3.5. Renewability Evaluation Study

The regeneration and reusability study is a significant factor for the adsorbent's applicability and economy. The recyclability of NFO-GO composites is investigated performing five adsorption/desorption cycles (Figure 13). The desorption of adsorbed MB dye is done at every cycle [59] from acetic/ethanolic solution after stirring for 12hrs at room temperature by magnetic stirrer. The adsorbent is reused for successive adsorption processes. It is noticed that adsorbent's adsorption capacity reduced in each consecutive cycle from 97.9% to 80.4% after the 5th cycle of the original adsorption capacity. After first cycle, the uptake capacity reduced down to 53% without desorption, that furthermore after the 5th cycle reduced to original value's 20.3%. The adsorption efficiency recovered effectively by ethanol/acetic acid solution desorption. The result indicated that NFO-GO composites can be a potential, efficient and cost effective adsorbent for MB removal because of attractive regeneration performance.

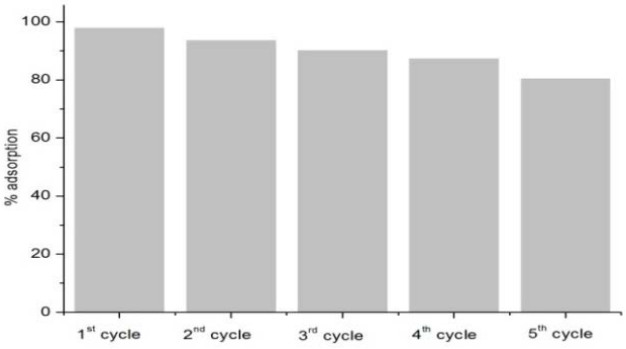

Figure 13. Reusability of NFO-GO for MB removal

4. Conclusion

The Methylene Blue dye adsorption is studied using $NiFe_2O_4$-Graphene Oxide composite. The study summarized as follows -

- Successful preparation of adsorbent NFO-GO was done as well as it has been suggested by the characterization study that it was nano range composite.
- Langmuir isotherm obeyed during the dye adsorption process with $97.94mgg^{-1}$ monolayer adsorption capacities.
- Second order kinetic model followed in the adsorption process.
- Nature of dye adsorptions is endothermic.
- There exists spontaneous interaction of NFO-GO-dye as well as controlled by Gibbs free energy reduction.
- pH sensitive dye adsorptions is observed.

Acknowledgements

We are thankful to NEHU, shilling, IITG Guwahati and USIC Gauhati University, IIAST for measuring TEM, XRD and Zeta potential respectively. We are also grateful

to the department of chemistry, B N College, Dhubri for allowing to carry out the experimental work.

References

[1] Lewis R.M., Andre-Schwartz J., Gs H., Ms H., *142 LCTA IN STUDY POPULATIONS.* vol. 21. 1978.

[2] Albert M., Lessin M.S. and Gilchrist B.F., "Methylene blue: Dangerous dye for neonates", *J Pediatr Surg*, 38. 1244-1245. 2003.

[3] Majithia A. and Stearns MP, "Methylene blue toxicity following infusion to localize parathyroid adenoma", *J Laryngol Otol*, 120. 138-140. 2006.

[4] Oz M., Lorke D.E. and Petroianu G.A., "Methylene blue and Alzheimer's disease", *Biochem Pharmacol*, 78. 927-932. 2009.

[5] Wang W., Cai K., Wu X., Shao X. and Yang X., "A novel poly(m-phenylenediamine)/reduced graphene oxide/nickel ferrite magnetic adsorbent with excellent removal ability of dyes and Cr(VI)", *J Alloys Compd*, 722. 532-43. 2017.

[6] Xiong W., Zeng G., Yang Z., Zhou Y., Zhang C., Cheng M., Liu Y., Hu L., Wan j., Zhou C., Xu R., and Li X., "Adsorption of tetracycline antibiotics from aqueous solutions on nanocomposite multi-walled carbon nanotube functionalized MIL-53(Fe) as new adsorbent", *Sci Total Environ*, 627. 235-244. 2018.

[7] Zhou C., Xu P., Lai C., Zhang C., Zeng G., Huang D., Cheng M., Hu L., Xiong W., Wen X., qin L., Yuan J., and Wang W., "Rational design of graphic carbon nitride copolymers by molecular doping for visible-light-driven degradation of aqueous sulfamethazine and hydrogen evolution" *Chem Eng J*, 359. 186-196. 2019.

[8] Al-Hamadani Y.A. J., Lee G., Kim S., Park C.M., Jang M., Her N., Han J., and Yoon Y., "Sonocatalytic degradation of carbamazepine and diclofenac in the presence of graphene oxides in aqueous solution", *Chemosphere*, 205. 719-727. 2018.

[9] Goodwin D.G., Adeleye A.S, Sung L., Ho K.T., Burgess R.M. and Petersen E.J., "Detection and Quantification of Graphene-Family Nanomaterials in the Environment", *Environ Sci Technol*, 52. 4491-4513. 2018.

[10] Deng X., Lü L., Li H. and Luo F., "The adsorption properties of Pb(II) and Cd(II) on functionalized graphene prepared by electrolysis method" *J Hazard Mater*, 183. 923-930. 2010.

[11] Bao N., Shen L., Wang Y., Padhan P., and Gupta A., "A facile thermolysis route to monodisperse ferrite nanocrystals", *J Am Chem Soc*, 129. 12374-12375. 2007.

[12] Hummers W.S. and Offeman R.E., "Preparation of Graphitic Oxide" *J Am Chem Soc*, 80. 1339. 1958.

[13] Ahmed T., Ali A.M. and Gupta S.S., "Application of NFO-GO composite for the removal of acid blue 25 toxic dye from aqueous solution", *Desalin Water Treat*, 174. 400-413. 2020.

[14] Cullity B.D. and Stock S.R. *Elements of X-RAY DIFFRACTION*, Plant Management & Physiology, Second Edition. 1978.

[15] Sivakumar P., Ramesh R., Ramanand A., Ponnusamy S. and Muthamizhchelvan C., "Synthesis and characterization of NiFe2O4 nanoparticles and nanorods", *J Alloys Compd*. 563. 6-11. 2013.

[16] Ferrari A.C., Meyer J.C., Scardaci V., Casiraghi C., Lazzeri M., Mauri F., Piscanec S., Jiang D., Novoselov K.S., Roth S. and Geim A.K., "Raman spectrum of graphene and graphene layers", *Phys Rev Lett* 97. 187401-187404. 2006.

[17] Rao C.N.R., Biswas K., Subrahmanyam K.S. and Govindaraj A., "Graphene, the new nanocarbon", *J Mater Chem*, 19. 2457-2469. 2009.

[18] Ahlawat A. and Sathe V.G., "Raman study of NiFe2O4 nanoparticles, bulk and films: Effect of laser power", *J Raman Spectrosc*, 42. 1087-1094. 2011.

[19] Kreisel J., Lucazeau G. and Vincent H., "Raman Spectra and Vibrational Analysis of BaFe12O19Hexagonal Ferrite", *J Solid State Chem*, 137. 127-137. 1998.

[20] Liu S.Q., Xiao B., Feng L.R., Zhou S.S., Chen Z.G., Liu C.B., Chen F., Wu Z.Y., Xu N. and Oh W.C., "Graphene oxide enhances the Fenton-like photocatalytic activity of nickel ferrite for degradation of dyes under visible light irradiation", *Carbon*, 64. 197-206. 2013.

[21] Xie G., Xi P., Liu H., Chen F., Huang L., Shi Y., Hou F., Zeng Z., Shau C. and Wang J., "A facile chemical method to produce superparamagnetic graphene oxide-Fe 3O 4 hybrid composite and its application in the removal of dyes from aqueous solution", *J Mater Chem*, 22. 1033-1039. 2012.

[22] Chen G., Sun M., Wei Q., Zhang Y., Zhu B. and Du B., "Ag3PO4/graphene-oxide composite with remarkably enhanced visible-light-driven photocatalytic activity toward dyes in water", *J Hazard Mater*, 244-245. 86-93. 2013.

[23] Oliveira L.C.A., Rios R.V.R.A., Fabris J.D., Garg V., Sapag K. and Lago R.M., "Activated carbon/iron oxide magnetic composites for the adsorption of contaminants in water" *Carbon*, 40. 2177-2183. 2002.

[24] Özcan A.S., Erdem B. and Özcan A., "Adsorption of Acid Blue 193 from aqueous solutions onto Na - bentonite and DTMA - bentonite", *J. Colloid Interface Sci.*, 280. 44-54. 2004.

[25] Ferrero F., "Dye removal by low cost adsorbents: Hazelnut shells in comparison with wood sawdust", *J Of Hazardous Mater*, 142.144-152. 2007.

[26] Lipatova I.M., Makarova L.I. and Yusova A.A., "Adsorption removal of anionic dyes from aqueous solutions by chitosan nanoparticles deposited on the fibrous carrier", *Chemosphere*, 212. 1155-1162. 2018.

[27] Sarma G.K., Sengupta S. and Bhattacharyya K.G., "Methylene Blue Adsorption on Natural and Modified Clays", *Sep Sci Technol*, 46. 1602-1614. 2011.

[28] Li Y., Du Q., Liu T., Sun J., Wang Y., Wu S., wang Z., Xia Y. and Xia L., "Methylene blue adsorption on graphene oxide/calcium alginate composites", *Carbohydr Polym*, 95. 501-507. 2013.

[29] Wu Z., Zhong H., Yuan X., Wang H., Wang L., Chen X., Zeng G. and Wu Y., "Adsorptive removal of methylene blue by rhamnolipid-functionalized graphene oxide from wastewater", *Water Res*, 67. 330-344. 2014.

[30] Chowdhury S., Mishra R., Saha P. and Kushwaha P., "Adsorption thermodynamics, kinetics and isosteric heat of adsorption of malachite green onto chemically modified rice husk", *Desalination*, 265. 159-168. 2011.

[31] Rahchamani J., Mousavi H.Z. and Behzad M., "Adsorption of methyl violet from aqueous solution by polyacrylamide as an adsorbent: Isotherm and kinetic studies", *Desalination*, 267. 256-260. 2011.

[32] Shukla A., Zhang Y.H., Dubey P., Margrave J.L. and Shukla S.S., "The role of sawdust in the removal of unwanted materials from water", *J Hazard Mater*, 95. 137-152. 2002.

[33] Ho Y.S., "Citation review of Lagergren kinetic rate equation on adsorption reactions", *Scientometrics*, 59. 171-177. 2004.

[34] Ho Y.S. and McKay G., "The kinetics of sorption of divalent metal ions onto sphagnum moss peat", *Water Res*, 34. 735-742. 2000.

[35] Chien S.H. and Clayton W.R., "Application of Elovich Equation to the Kinetics of Phosphate Release and Sorption in Soils", *Soil Sci Soc Am J*, 44. 265-268. 1980.

[36] Dawood S. and Sen T.K., "Removal of anionic dye Congo red from aqueous solution by raw pine and acid-treated pine cone powder as adsorbent: Equilibrium, thermodynamic, kinetics, mechanism and process design", *Water Res*, 46. 1933-1946. 2012.

[37] McKay G., Blair H.S. and Gardner J., "The adsorption of dyes in chitin. III. Intraparticle diffusion processes", *J Appl Polym Sci*, 28. 1767-1778. 1983.

[38] Walter J. Weber and J. Carrell Morris., "Kinetics of Adsorption on Carbon from Solution", *J Sanit Eng Div*, 89. 31-60. 1963.

[39] Tang H., Zhou W. and Zhang L., "Adsorption isotherms and kinetics studies of malachite green on chitin hydrogels", *J Hazard Mater*, 209-210. 218-225. 2012.

[40] Boyd G.E., Adamson A.W. and Myers L.S., "The Exchange Adsorption of Ions from Aqueous Solutions by Organic Zeolites. II. Kinetics", *J Am Chem Soc*, 69. 2836-2848. 1947.

[41] Chao T.T., Harward M.E. and Fang S.C., "Adsorption and Desorption Phenomena of Sulfate Ions in Soils", *Soil Sci Soc Am J*, 26. 234-237. 1962.

[42] Kinniburgh D.G., "General Purpose Adsorption Isotherms", *Environ Sci Technol*, 20. 895-904. 1986.

[43] Chowdhury S., Mishra R., Saha P. and Kushwaha P., "Adsorption thermodynamics, kinetics and isosteric heat of adsorption of malachite green onto chemically modified rice husk", *Desalination*, 265. 159-168. 2011.

[44] Weber T.W. and Chakravorti R.K., "Pore and solid diffusion models for fixed-bed adsorbers", *AIChE J*, 20. 228-238. 1974.

[45] Hameed B.H., "Equilibrium and kinetic studies of methyl violet sorption by agricultural waste", *J Hazard Mater*, 154. 204-212. 2008.
[46] Wu Y., Luo H., Wang H., Wang C., Zhang J. and Zhang Z., "Adsorption of hexavalent chromium from aqueous solutions by graphene modified with cetyltrimethylammonium bromide", *J Colloid Interface Sci*, 394. 183-191. 2013.
[47] Travis C.C. and Etnier E.L., "A Survey of Sorption Relationships for Reactive Solutes in Soil", *J Environ Qual*, 10. 8-17. 1981.
[48] Hutson N.D. and Yang R.T., "Theoretical basis for the Dubinin-Radushkevitch (D-R) adsorption isotherm equation", *Adsorption*, 3. 189-195. 1997.
[49] Aksoyoglu S., "Sorption of U(VI) on granite", *J Radioanal Nucl Chem Artic*, 134. 393-403. 1989.
[50] Hussain S., van Leeuwen J., Chow C., Beecham S., Kamruzzaman M., Wang D., Drikas M. and Aryal R., "Removal of organic contaminants from river and reservoir waters by three different aluminum-based metal salts: Coagulation adsorption and kinetics studies", *Chem Eng J*, 225. 394-405. 2013.
[51] Arami M., Yousefi Limaee N. and Mahmoodi N.M., "Investigation on the adsorption capability of egg shell membrane towards model textile dyes", *Chemosphere*, 65. 1999-2008. 2006.
[52] Gupta S. and Bhattacharyya K., "Using aqueous kaolinite suspension as a medium for removing phosphate from water", *Adsorpt Sci Technol*, 30. 533-547. 2012.
[53] Luo P., Zhao Y., Zhang B., Liu J., Yang Y. and Liu J., "Study on the adsorption of Neutral Red from aqueous solution onto halloysite nanotubes", *Water Res*, 44. 1489-1497. 2010.
[54] Tan I.A.W., Ahmad A.L. and Hameed B.H., "Adsorption isotherms, kinetics, thermodynamics and desorption studies of 2,4,6-trichlorophenol on oil palm empty fruit bunch-based activated carbon", *J Hazard Mater*, 164. 473-482. 2009.
[55] Fu J., Chen Z., Wang M., Liu S., Zhang J., Zhang J., Han R. and Xu q., "Adsorption of methylene blue by a high-efficiency adsorbent (polydopamine microspheres): Kinetics, isotherm, thermodynamics and mechanism analysis", *Chem Eng J*, 259. 53-61. 2015.
[56] Wu Z., Zhang L., Guan Q., Ning P. and Ye D., "Preparation of α-zirconium phosphate-pillared reduced graphene oxide with increased adsorption towards methylene blue", *Chem Eng J*, 258. 77-84. 2014.
[57] Wang Y., Wang W. and Wang A., "Efficient adsorption of methylene blue on an alginate-based nanocomposite hydrogel enhanced by organo-illite/smectite clay", *Chem Eng J*, 228. 132-139. 2013.
[58] Liu Y., Wang J., Zheng Y. and Wang A., "Adsorption of methylene blue by kapok fiber treated by sodium chlorite optimized with response surface methodology", *Chem Eng J*, 184. 248-255. 2012.
[59] Rachna K., Agarwal A. and Singh N.B., "Preparation and characterization of zinc ferrite—Polyaniline nanocomposite for removal of rhodamine B dye from aqueous solution", *Environ Nanotechnology, Monit Manag*, 9. 154-163. 2018.

Supplementary File (Figure)

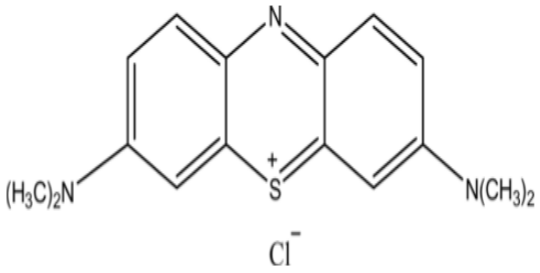

Figure S1. Structure of Methylene Blue(MB).

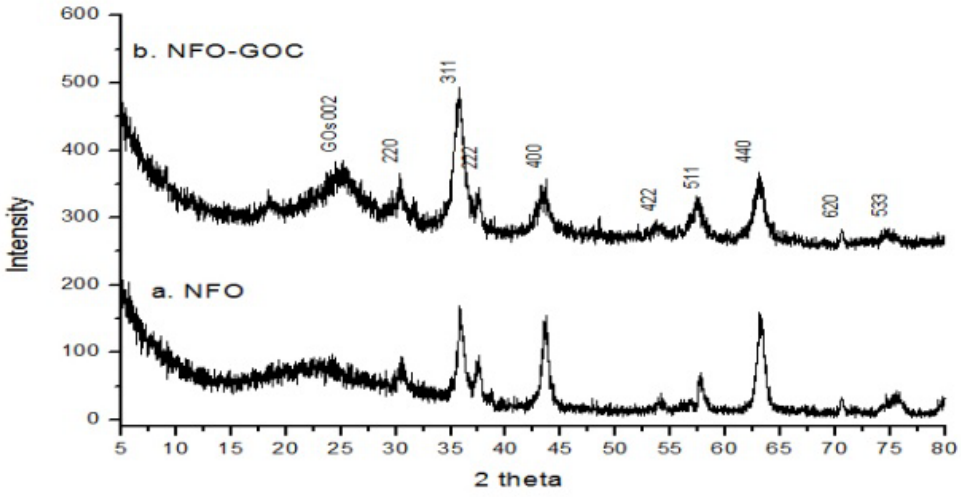

Figure S2. X-Ray diffraction pattern of (a) NFO (b) NFO-GO

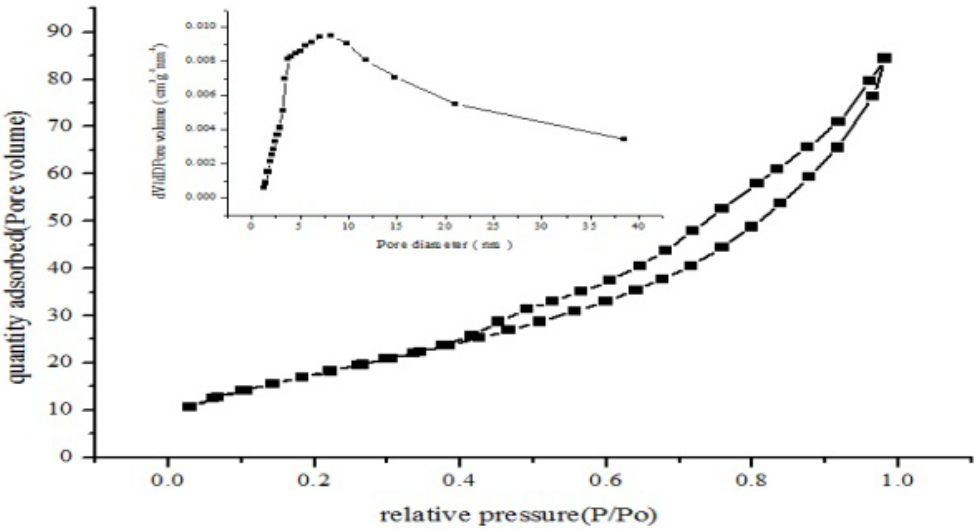

Figure S3. Nitrogen isotherm and pore size distribution of NFO-GO composite

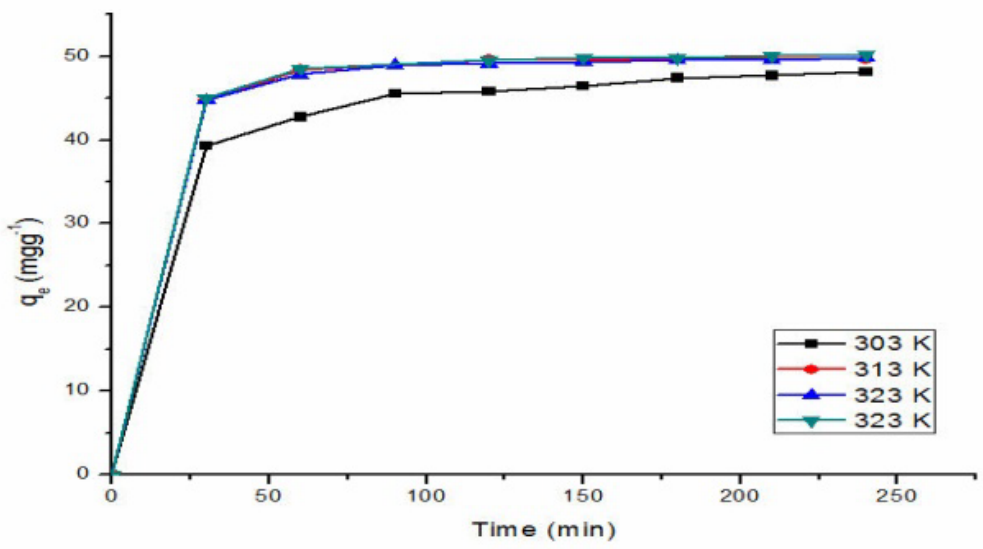

Figure S4. Influence of time of MB adsorption onto NFO-GO composite

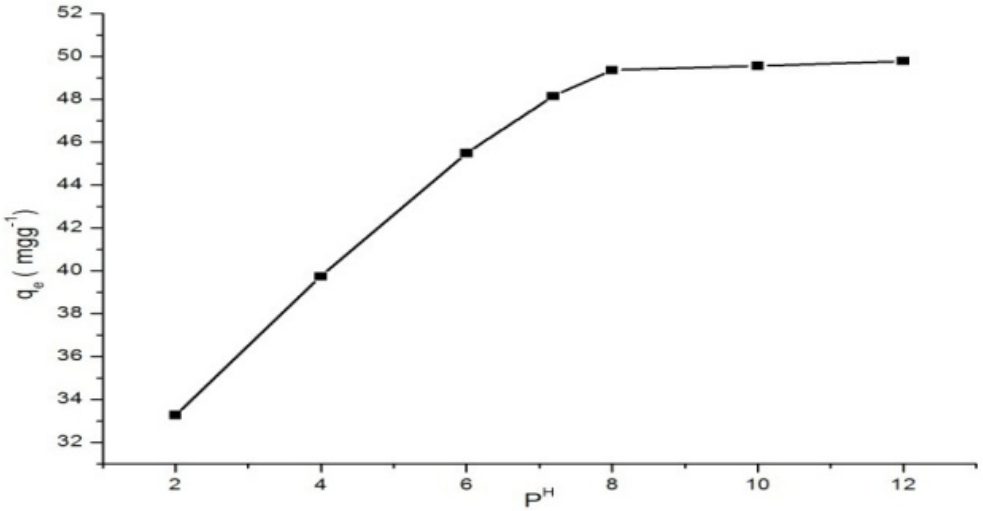

Figure S5. Influence of P^H of MB adsorption onto NFO-GO composite

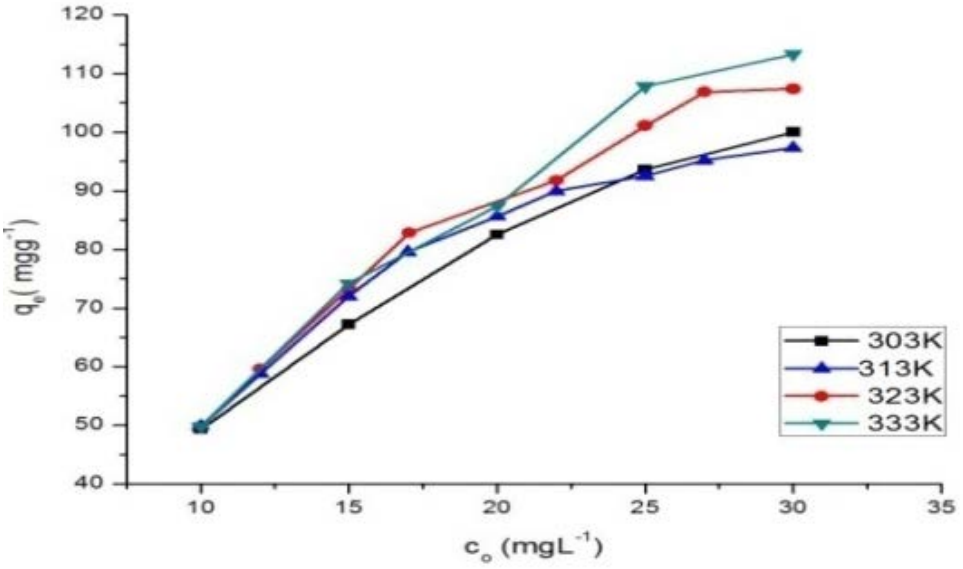

Figure S6. Influence of concentration of MB adsorption onto NFO-GO composite.

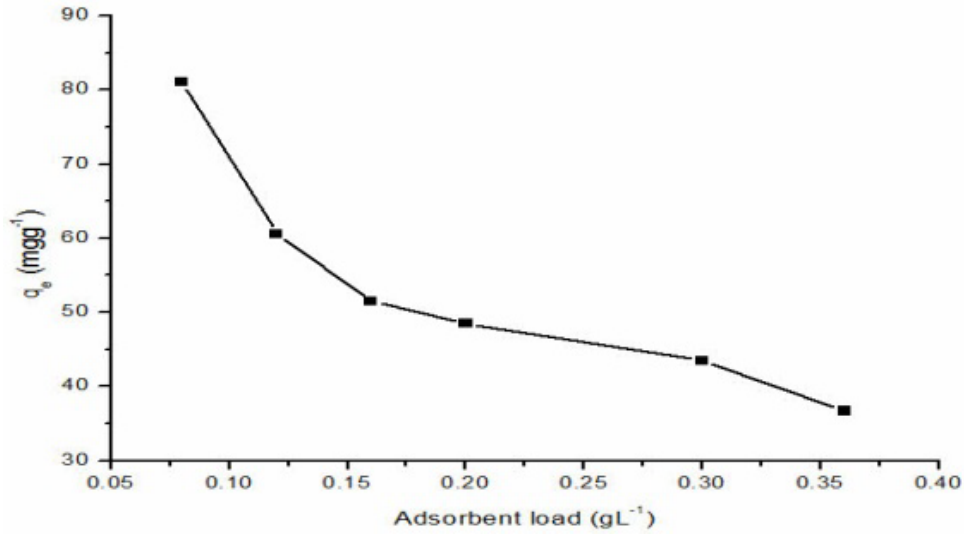

Figure S7. Influence of adsorbent dosages on MB adsorption onto NFO-GO composite

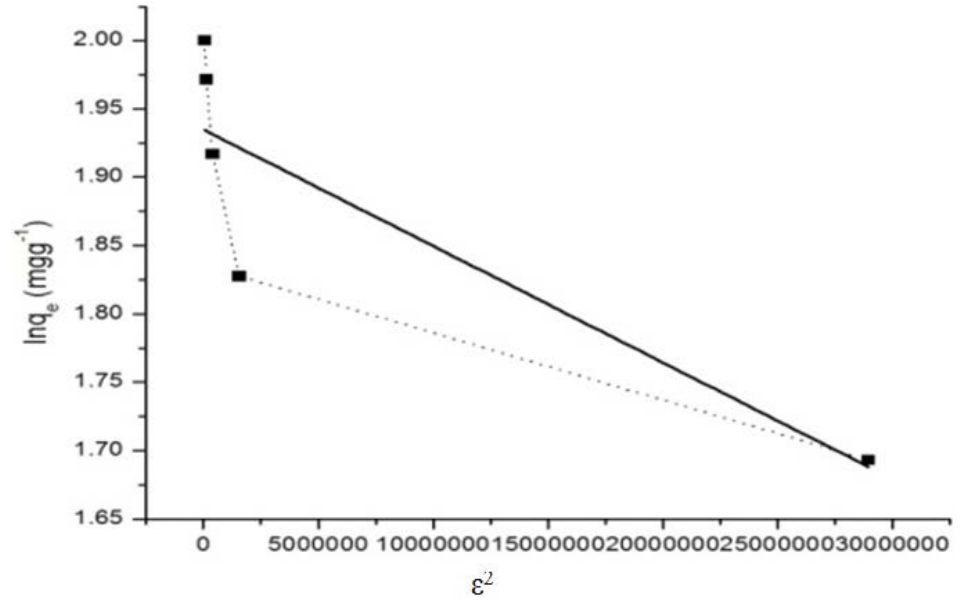

Figure S8. Dubinin-Radushkevich isotherm model of MB adsorption onto NFO-GO composite

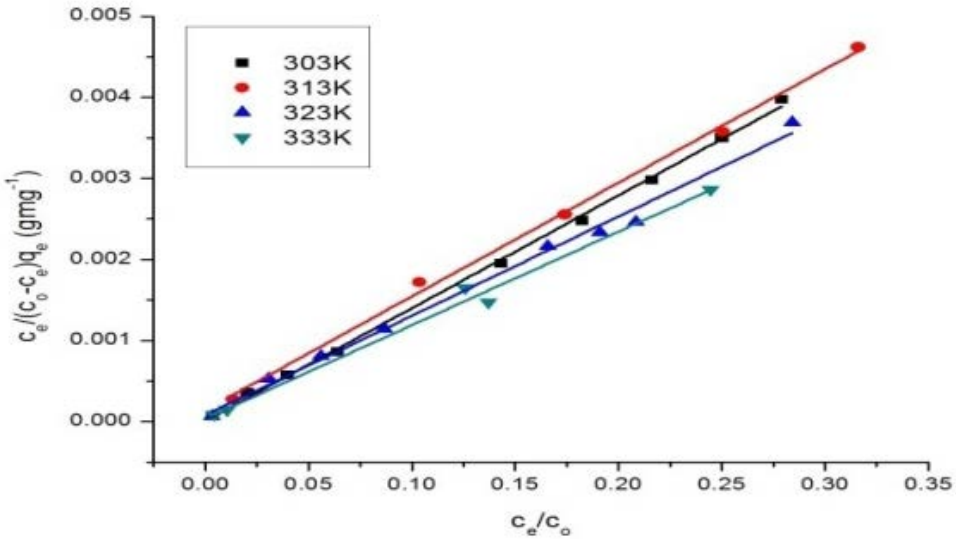

Figure S9. BET isotherm model of MB adsorption onto NFO-GO composite